ADVANCED MATERIALS INTERFACES
Open Access
www.advmatinterfaces.de

Plasma-Based Synthesis of Freestanding Graphene from a Natural Resource for Sensing Application

*M. Adeel Zafar, Yang Liu, Francisco C. Robles Hernandez, Oomman K. Varghese, and Mohan V Jacob**

Atmospheric pressure microwave plasma has the lead in synthesizing freestanding and scalable graphene within seconds without the need for high vacuum and temperature. However, the process is limited in utilizing chemical sources for synthesis, such as methane and ethanol. Herein, the usage of an extract of a sustainable precursor, that is, *Melaleuca alternifolia*, commonly known as tea tree, is for the first time reported to synthesize graphene nanosheets in atmospheric pressure microwave plasma. The synthesis is carried out in a single step at a remarkably low microwave power of 200 W. The morphology, structure, and electrochemical properties of graphene are studied using state-of-the-art characterization techniques such as Raman spectroscopy, X-ray diffraction, transmission electron microscopy (TEM) and electrochemical impedance spectroscopy. The TEM images reveal the presence of a combination of nanostructures such as nano-horns, nano-rods, or nano-onions consisting of multi-layer graphitic architectures. An excellent sensing capability of as-synthesized graphene is demonstrated through the detection of diuron herbicide. A commendable linear range of 20 µM to 1 mM and a limit of detection of 5 µM of diuron is recorded.

1. Introduction

Graphene has been greatly applauded in academia and industry owing to its extraordinary properties and myriad applications.[1,2] Characterized by a single layer of graphite, graphene is composed of sp^2-bonded carbon atoms arranged in a honeycomb lattice structure.[3] Multiple techniques have been developed to synthesize graphene, mainly classified as top–down and bottom–up approaches. The bottom-up approach, that is, modified Hummers' method, is a well-established chemical synthesis technique to synthesize graphene. However, this technique, not only utilizes strong acids and oxidants[4,5] but also entails numerous steps of synthesis such as dilution, mixing, oxidation, reduction, washing, centrifuging, and intense stirring.[6] On the other hand, some of the bottom–up methods, in particular, chemical vapor deposition (CVD) and plasma-enhanced chemical vapor deposition (PE-CVD) are expensive and laborious methodologies comprising pre-synthesis and post-synthesis requirements, that is, high vacuum, pre-heating, and subsequent transfer of graphene to other substrates.[7–9] Recently, a new bottom-up approach, so-called atmospheric pressure microwave plasma (APMP) is gaining popularity as it synthesizes graphene without the hassles of pre-heating, high vacuuming, and the need for a substrate. Most importantly, the graphene obtained through this method happens to be freestanding and scalable.[10,11]

The precursors used for producing graphene have a significant role in determining the sustainability of the synthesis process. Often graphene is produced from commercially available graphite,[12] graphene oxide (GO),[13] methane, or other unreplenishable hydrocarbons.[14] These resources

M. A. Zafar, M. V. Jacob
Electronics Materials Lab
College of Science and Engineering
James Cook University
Townsville, Queensland 4811, Australia
E-mail: mohan.jacob@jcu.edu.au
Y. Liu
College of Science and Engineering
James Cook University
Townsville, Queensland 4811, Australia
The ORCID identification number(s) for the author(s) of this article can be found under https://doi.org/10.1002/admi.202202399.

DOI: 10.1002/admi.202202399

F. C. R. Hernandez
Mechanical Engineering Technology
College of Technology
University of Houston
Houston, TX 77204-4020, USA
O. K. Varghese
Nanomaterials and Devices Laboratory
Department of Physics
University of Houston
Houston, TX 77204, USA
O. K. Varghese
Texas Center for Superconductivity
University of Houston
Houston, TX 77204, USA

are generally non-renewable, expensive, and/or produce toxic chemicals during synthesis practice. This has driven scientists to replace these precursors with economical, regenerative, and environment-friendly raw materials. Considerable attempts have been made to derive graphene from a wide range of natural resources, for example, food materials, botanical hydrocarbons, and biomass.[15] These include table sugar, honey, butter,[16] cookies, chocolate,[17] camphor,[18] tea tree essential oil,[19] *Citrus sinensis* oil,[20] soybean oil,[21] waste cooking palm oil,[22] nutshells,[21] *Colocasia esculenta*, and *Nelumbo nucifera* leaves.[23] However, the usage of these feedstocks is limited to certain methods, such as modified Hummers' method, pyrolysis, and CVD or PE-CVD techniques. On the other hand, for APMP, the use of sustainable precursors has not been reported yet. The APMP technique is mainly associated with ethanol[24–29] and methane resources.[30] These precursors are extracted from non-renewable bases and are mostly explosive or toxic. In addition, it has been observed that the increase in the feed of ethanol above a certain quantity causes an extinction of plasma flame,[31] which eventually limits the production rate of graphene.

A hydrocarbon-rich and naturally occurring resource, *Melaleuca alternifolia*, has the potential to be an excellent alternative precursor for graphene synthesis. Commonly known as tea tree, it is an abundant and cost-effective resource. It comprises more than 100 compounds, which include terpinen-4-ol ($C_{10}H_{18}O$, 30–48%), γ-terpinene ($C_{10}H_{16}$, 10–28%), α-terpinene ($C_{10}H_{16}$, 5–13%), and 1, 8-cineole ($C_{10}H_{18}O$, 0–15%) as primary constituents and some other compounds in trace amounts.[19] The chemical formula, that is, $C_{28}H_{60}O_4P_2S_4Zn$, given by PubChem also shows the presence of an ample amount of hydrocarbons. Previously, this resource has been used for graphene synthesis in the PE-CVD technique; though the actual synthesis was quick, the overall synthesis was time-consuming due to the heating and cooling required and was substrate-dependant.[19]

This study aimed to synthesize graphene through a facile, rapid, viable, and environmentally benign process. We synthesized free-standing graphene from *M. alternifolia* extract using the APMP. To the best of our knowledge, this is the first report on the APMP synthesis of graphene from a sustainable parent material. The graphene was synthesized at a remarkably low microwave power of 200 W in ambient air. As the practical use of graphene synthesized through APMP is scarcely reported, herein we also demonstrate the employment of as-fabricated graphene for diuron herbicide detection.

2. Experimental Section

2.1. Materials

M. alternifolia was purchased from Australian Botanical Products (ABP, Victoria, Australia). Sodium dihydrogen orthophosphate ($NaH_2PO_4.2H_2O$), disodium hydrogen orthophosphate (Na_2HPO_4), sodium hydroxide (NaOH), potassium hexacyanoferrate (III) $K_3[Fe(CN)_6]$, potassium chloride (KCl), and diuron were obtained from Sigma–Aldrich, Australia. All chemicals were used as received without any further treatment. Ultrapure water was used throughout all the experiments.

2.2. Synthesis of Graphene

The graphene nanosheets were synthesized using a downstream APMP, schematically shown in **Figure 1**a. A 2.45 GHz microwave with a variable output power of maximum of 2 kW was used to generate plasma. The discharge took place inside a quartz tube having an external diameter of 30 mm. The investigated microwave powers were set at the values of 200, 400, and 600 W. A custom-made precursor delivery system was made to transport the carbon precursor, that is, tea tree oil vapors into the quartz chamber. The tea tree oil vapors were conveyed into the chamber along with argon gas (plasma gas) at the optimum flow rate of 3 slm. Upon exposure to the plasma, the tea tree vapors first decomposed into constituent elements and then started arranging in a graphene structure. The synthesis stages are shown schematically in Figure 1b. The graphene nanosheets were directly deposited on the silicon substrate for characterizations. The synthesis parameters provided here were optimal values, obtained after a series of experiments. The reproducibility of the synthesis at optimum conditions was also verified through seven replicates.

The graphene's morphology and structural investigation were carried out using scanning electron microscopy (SEM) (Hitachi

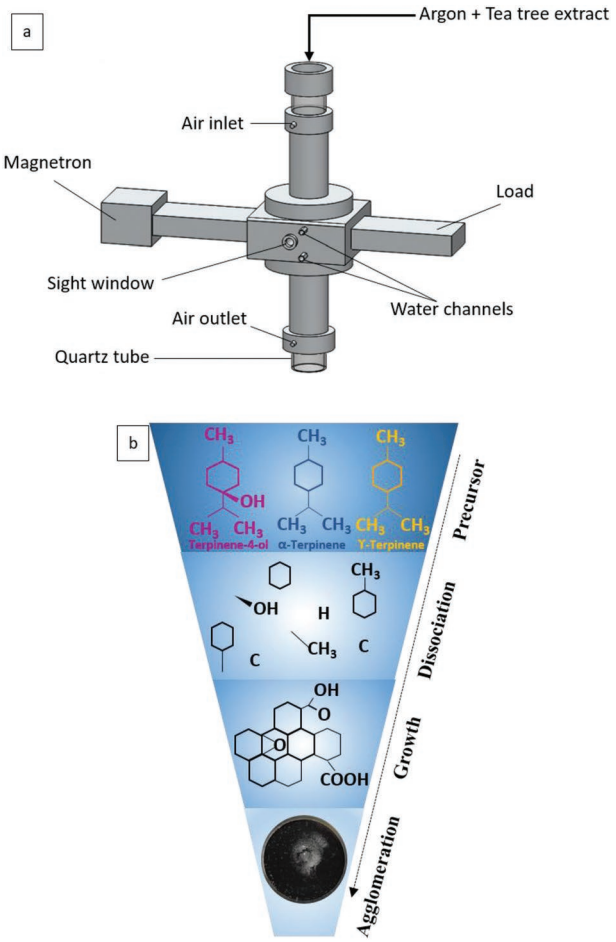

Figure 1. a) A diagrammatic representation of atmospheric pressure microwave plasma reactor. b) Schematic illustration of steps involved in the synthesis of graphene inside the reactor.

SU 5000) and confocal laser Raman spectroscopy (Witec, 532 nm laser). Rigaku Smart Lab X-ray diffractometer was used for X-ray diffraction (XRD). The X-ray photoelectron spectroscopy (XPS) studies were performed using a Kratos Axis Ultra XPS with an Al Kα X -ray source. The JEOL 2100 F machine operated at 200 kV was used for transmission electron microscopy (TEM) images.

2.3. Electrochemical Measurements

Electrochemical measurements were performed on Palm Sense 4 (Palm Instruments, Netherlands) potentiostat using the three-electrode system with a glassy carbon electrode (GCE) as a working electrode, a platinum wire as the counter electrode, and an Ag/AgCl as the reference electrode. Before each testing or modification, the bare GCE was first mechanically polished with 0.3 and 0.05 µM alumina slurry, followed by ultrasonic cleaning in ethanol and ultrapure water, respectively. To prepare a modified electrode, 10 µL of graphene (1 mg mL^{-1}) aliquot was drop-casted on GCE and dried at room temperature. Such an electrode was denoted as graphene/GCE. The electrochemical impedance spectroscopy (EIS) experiment was conducted in 0.1 M KCl containing 5 mM $K_3[Fe(CN)_6]$ solution in the frequency swept from 0.1 Hz to 100 kHz. Cyclic voltammetry (CV) and differential pulse voltammetry (DPV) were carried out in 0.1 M phosphate buffer solution (PBS) (pH 7.0) containing a certain amount of diuron.

3. Results and Discussion

Raman spectroscopy is a non-destructive tool for the structural elucidation of carbon materials. Therefore, graphene samples prepared at 200, 400, and 600 W were analyzed using Raman spectroscopy. All Raman results showed three vibrational modes related to graphene materials. D peak at ≈1335 cm^{-1} corresponded to the defect mode, G peak at ≈1570 cm^{-1} implicated vertical vibration mode, and a 2D peak at ≈2677 cm^{-1} indicated two-phonon vibration mode.[32]

The Raman results exhibited in **Figure 2**a show the increase in the intensity of the D peak with the increase of microwave power. The D peak reflects the structural imperfections in the graphene materials. Mainly, it is associated with the functional groups attached to the basal plane of graphene.[33] However, it is also ascribed to the defects such as vacancies, edge defects, bond-angle disorder, and bond-length disorder.[34] In the current work, the lowest power, that is, 200 W shows a comparatively smaller value of I_D/I_G in the sample (shown in Figure 2b); hence, indicating fewer disorders or higher oxygen content attached to the 200 W graphene structure.

Generally, the 2D peak is considered a significant feature in the Raman spectra of graphene-related materials. The intensity ratio between 2D and G peaks, that is, I_{2D}/I_G and full width at half-maximum (FWHM) of the 2D peak are normally associated with the number of layers in graphene. In literature, the I_{2D}/I_G ratio of 1 to 1.5 with FWHM ≈ 50 cm^{-1}, and I_{2D}/I_G of 2 or higher with FWHM ≈ 30 cm^{-1} are usually linked with the bilayer and monolayer structures, respectively.[35,36] In this study, the 200 W sample exhibited I_{2D}/I_G and FWHM values of 1.04 and 56 cm^{-1}, respectively, suggestive of few to multi-layer graphene. Slightly broader 2D peaks of 400 and 600 W samples, having FWHM of 62 cm^{-1} and 65 cm^{-1} respectively, and relatively smaller I_{2D}/I_G values were indicative of the higher number of layers in comparison to the 200 W sample. Thus, the remaining investigations and applications were studied using a 200 W graphene sample.

XPS was performed on the 200 W graphene sample to unravel their elemental composition and functional group species. The XPS survey scans given in **Figure 3**a clearly exhibit the presence of C and O in the sample having the composition of ≈87% and ≈10% respectively. The peaks centered at 284 and 531.5 eV were ascribed to C1s and O1s respectively. To understand the bonding structures of C and O elements, the high-resolution spectra of C1s and O1s were analyzed comprehensively.

The high-resolution spectrum of C1s with deconvoluted peaks is given in Figure 3b. Overall, four component peaks were identified in the spectrum. The key peaks at 284.3 and 285 eV corresponded to sp^2—C and sp^3—C, respectively. The

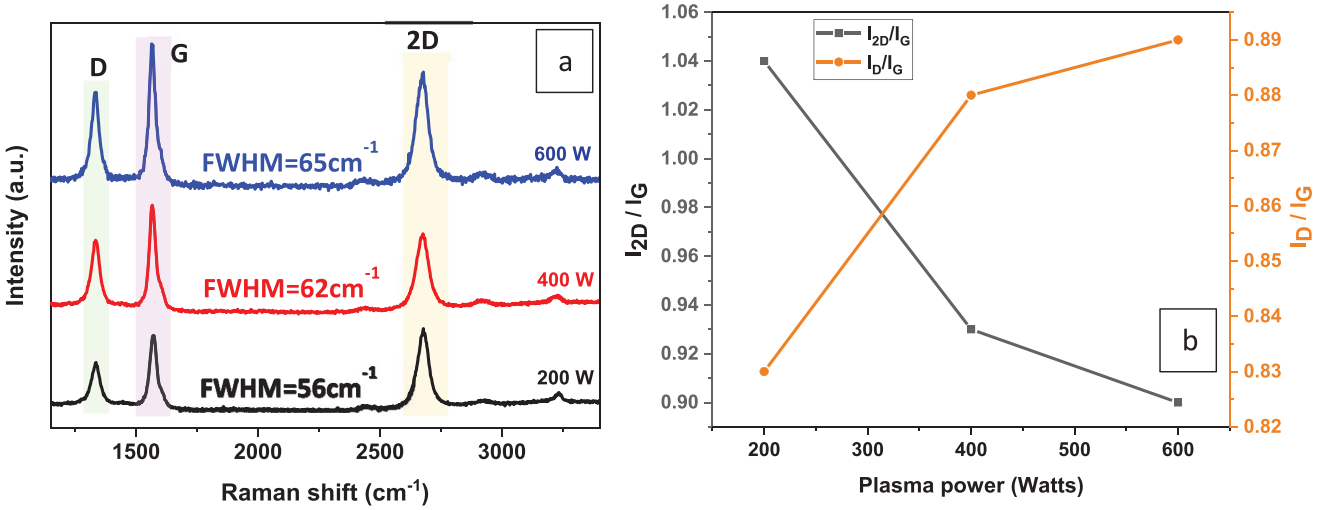

Figure 2. a) Raman spectra and b) peaks' intensity ratios of graphene samples synthesized at different microwave powers.

ADVANCED MATERIALS INTERFACES
Open Access
www.advmatinterfaces.de

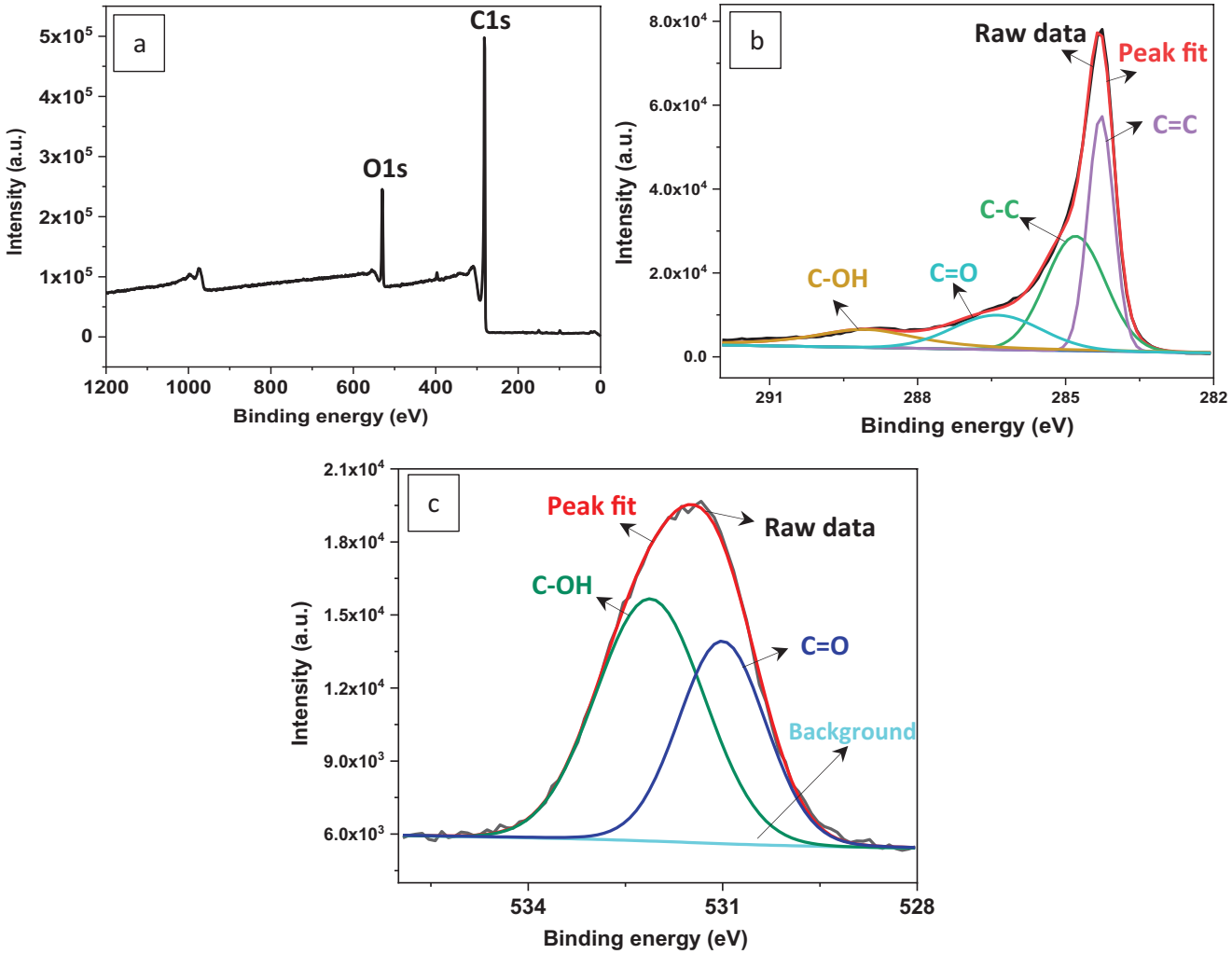

Figure 3. a) Survey scan XPS spectrum of 200 W graphene sample, and deconvoluted peaks of high-resolution b) C1s and c) O1s XPS spectra.

peak at 286.4 eV reflects C=O, whereas the smallest peak at 289 eV represents C−OH bonding. The occurrence of sp^2−C is suggestive of the conjugated honeycomb lattice arrangement of graphene, while sp^3−C indicates substitution defects in graphene or the edges of the graphene nanosheets.[37] The high-resolution spectra of O1s (Figure 3c) showed contributions at 531 and 532.1 eV arising from C=O and C−OH respectively. Comparing our XPS results with that of Lambert et al.,[38] where they also used atmospheric pressure microwave plasma, it was found that they obtained a fairly low amount of oxygen, that is, 3%. However, their synthesis was from graphene oxide at a quite high power of 900 W.

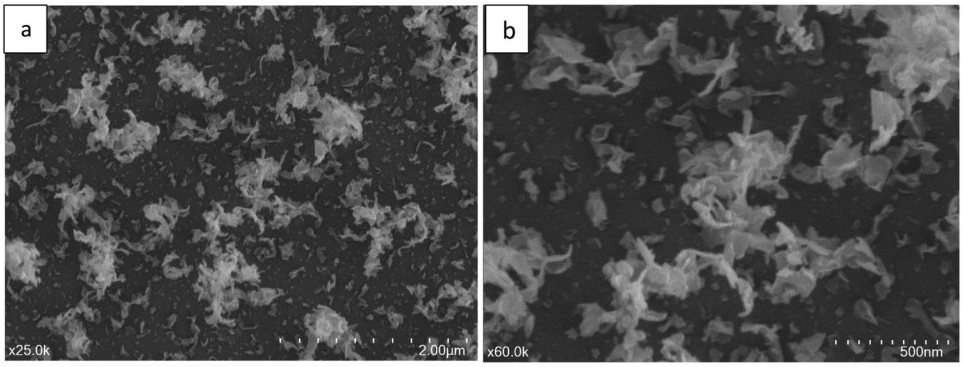

Figure 4. SEM images of 200 W graphene sample at a) lower and b) higher magnification.

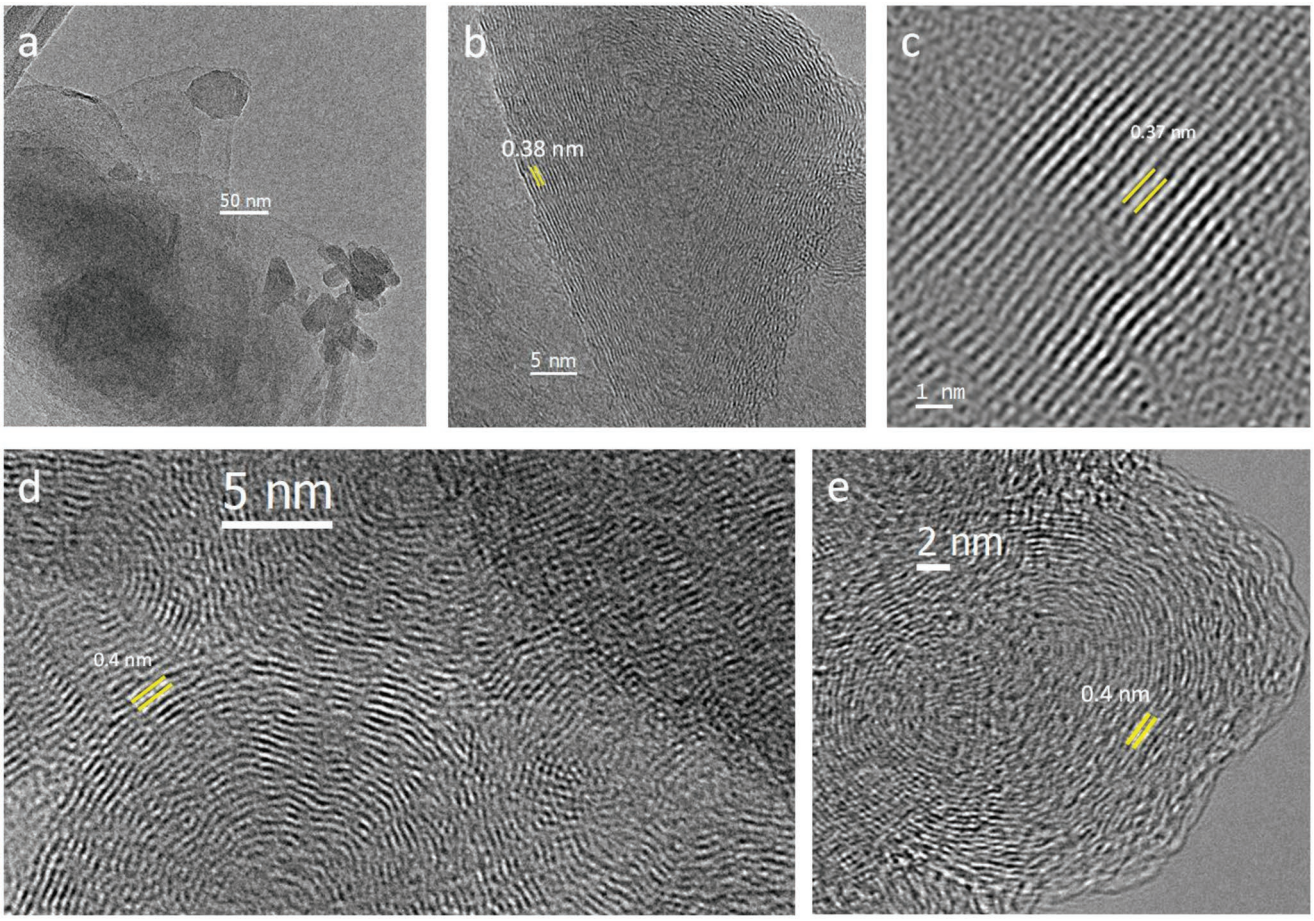

Figure 5. Transmission electron microscopy of graphitic particles a) low magnification, b–e) HRTEM.

The graphene yield as a carbon material was also determined. The theoretical yield of carbon, that is, 46.9% was calculated in the tea tree oil (chemical formula $C_{28}H_{60}O_4P_2S_4Zn$). The breakdown of tea tree oil in the microwave plasma generated various carbon species, such as CO, CO_2, and CH,[39] which contributed to ≈23% of the total yield of graphene.

SEM images of the 200 W graphene sample taken at lower and higher magnifications are given in **Figure 4**. Figure 4a shows the dense accumulation of graphene nanosheets at varying places, where nanosheets coalesce together to form an aggregate. The aggregation can be attributed to the continuous synthesis process in which nanosheets after formation tend to reside on existing graphene nanosheets. A higher magnification image in Figure 4b reveals a typical vertically standing petal-like structure where graphene nanosheets are curled, wrinkled, and overlapped. The size of individual nanosheets varies between 50 and 150 nm. The morphology of the graphene is in good agreement with previous reports on graphene, where they have synthesized graphene from different resources.[40,41]

The low-magnification TEM images show a mix of regular nanoparticles and sheets. The TEM results agree with the idea of agglomerations of carbon nanostructures. The nanosheets are discernible in the TEM image (**Figure 5**a), supporting the SEM results presented in Figure 4. The sheets are potentially agglomerations of single- or multi-layered graphitic structures formed during the plasma synthesis, which turn into multi-layer architectures as seen in high-resolution TEM (HRTEM) (Figure 5c). In the case of Figure 5c, the graphitic particles observed have ≈20 layers. Graphene sheets with less number of layers are also observed. However, in most cases, the graphene sheets are multi-layered. The particles showing

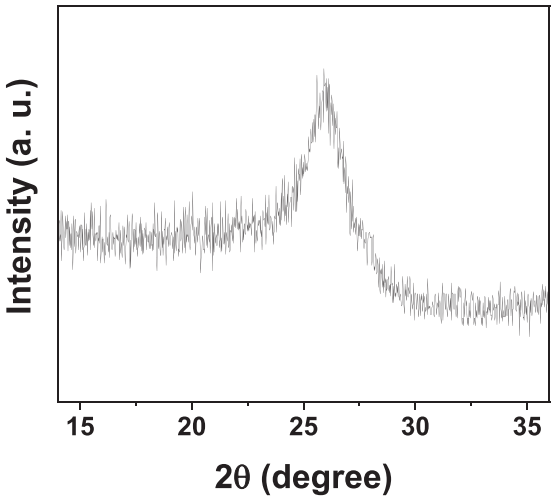

Figure 6. XRD pattern of 200 W graphene.

Table 1. Comparison of tea tree oil-derived graphene with others synthesized in atmospheric pressure microwave plasma.

Precursor	Microwave power [W]	Precursor flow rate [sccm]	I_D/I_G	Number of layers	Production rate [mg min^{-1}]	Ref.
Ethanol	250	0.3	–	Mono-and bi-layers	2	[10,25]
Ethanol	900	0.5–3.5	–	Few layers	2	[51]
Ethanol	200	0.0036	0.6	Multilayers	0.07	[52]
Ethanol	300	0.33	0.24	Few layers	1.33	[24]
Ethanol	300	0.048	0.35	Few to multilayers	1.45	[53]
Methane	1000	2–8	0.62	Multilayers	–	[30]
Methane	1200–1400	–	1.57 or 1.77	Few to multilayers	–	[54]
Tea tree oil	200	0.3	0.83	Multilayers	1.37	Current work

regular structures are multi-layer graphitic architectures with a variety of structures such as nano-horns, nano-rods (Figure 5b), or nano-onions (Figure 5d,e). The d spacing in all the structures is larger than the typical 0.33 nm.[42–44] The measured d spacing varies from 0.37 to 0.4 nm. This larger d spacing has already been reported in other structures such as morphed graphene.[45–47] In the present work, the rather smaller d spacing is commonly seen in the graphitic sheets, while the larger d spacing is typical of regular structures such as nano-horns, nano-rods, and nano-onions. Potentially, the nano-sheets with a d spacing of ≈0.37 nm are due to potential agglomerations of graphene sheets. However, the d spacing on the regular structures is attributed to the potential bending of the graphene sheets or the functional groups (C—OH, C=O, etc.) detected with XPS.

Crystalline materials have a unique XRD pattern that can be used as a fingerprint for materials identification. The distinctive peak centered at a diffraction angle (2θ) of 25.8° in **Figure 6** XRD pattern confirms the successful formation of the graphitic lattice. The peak position is associated with the (002) basal plane and corresponds to an interlayer spacing of 0.37 nm which is also verified by TEM. The interlayer spacing is higher compared to the typical 0.33 nm reported for graphene.[42–44,48] We attribute this to intercalated C=O and C—OH functional groups within the layers. Our XRD results are in good agreement with the other reports,[49,50] where they synthesized graphene using ultra-sonic exfoliation or hydrothermal methods. The comparable properties of tea tree-derived graphene (given in **Table 1**) make our synthesis approach a viable, cost-effective, and environmentally friendly strategy to replace unsustainable and harmful parent materials.

4. Application of Graphene in an Electrochemical Sensor

The electron-transfer kinetics of the graphene/GCE were investigated by comparing it with bare GCE using the EIS method. **Figure 7** shows the typical Nyquist plots of both electrodes. A semicircle region at higher frequencies attributed to the charge-transfer resistance (R_{ct}) and a linear region at lower frequencies corresponding to the diffusion process was observed for both electrodes.[55,56] The *R*ct values could be estimated by fitting the plot with an equivalent Randles circuit (inset, Figure 7), which was 206 and 79 Ω on the bare GCE and graphene/GCE, respectively. The substantial decrease in the R_{ct} of graphene/GCE by a

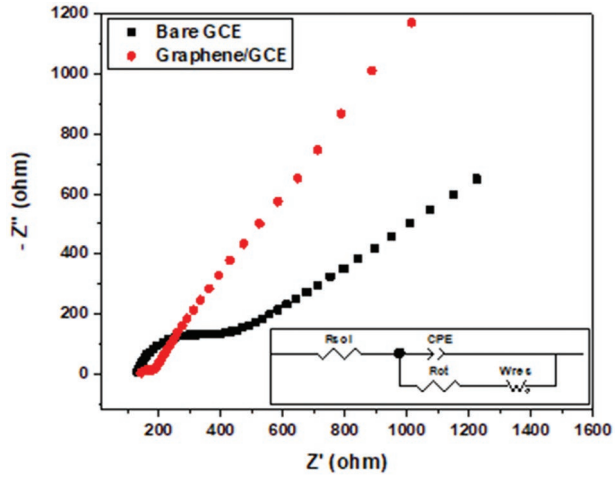

Figure 7. EIS of bare and graphene-modified GCE in 0.1 M KCl containing 5 mM $K_3[Fe(CN)_6]$. Frequency range 0.1 Hz to 100 kHz.

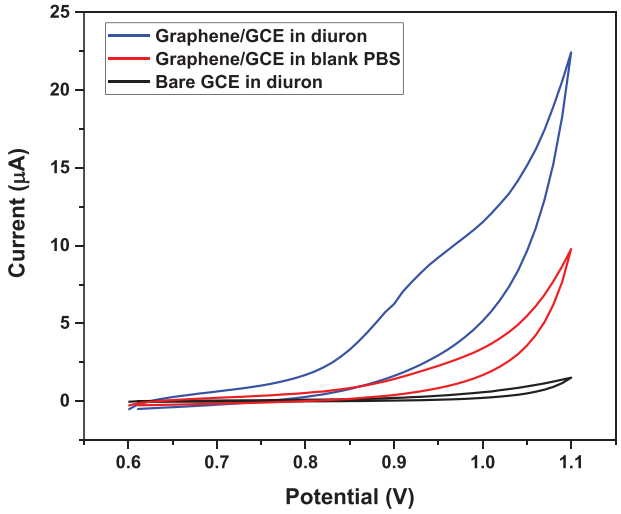

Figure 8. Cyclic voltammograms of bare and graphene-modified GCE in 0.1 M PBS containing 2 mM diuron and graphene/GCE in blank 0.1 M PBS; the scan rate is 10 mV s^{-1}.

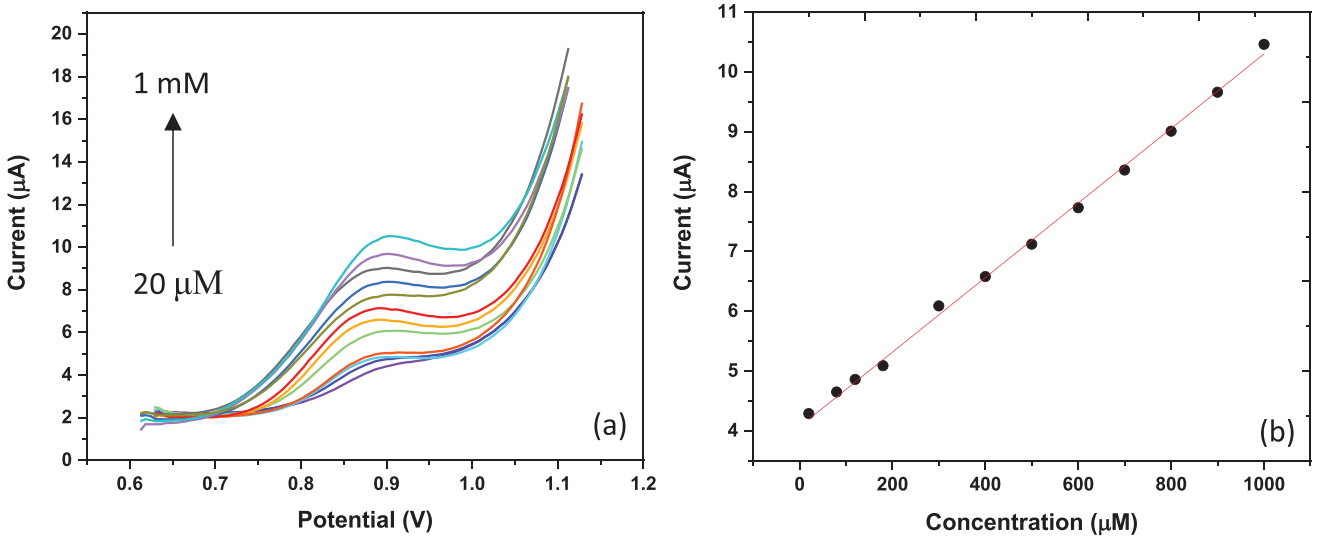

Figure 9. a) DPV curves at graphene/GCE for different concentrations (20, 80, 120, 180, 300, 400, 500, 600, 700, 800, 900, and 1000 μM) of diuron in 0.1 M PBS. b) Calibration plot from the DPV measurements.

factor of ≈2.6 times suggests the fast electron-transfer kinetics due to the excellent electro-conductibility of the graphene material.

The electrocatalytic activity of the graphene material for the detection of diuron was investigated in 0.1 M PBS (pH 7.0) containing 2 mM diuron using CV. **Figure 8** indicates that the electrochemical reaction of diuron at the bare GCE undergoes a sluggish charge-transfer kinetic process. However, the graphene/GCE electrode improved the peak current substantially. The diuron undergoes an irreversible chemical reaction and forms a dimmer resultantly.[57] The graphene/GCE performance in the absence of diuron showed a different voltammogram with no peak formation. Similar cyclic voltammograms were observed by Wong et al.[58] and Morita et al.[59] in separate studies for diuron detection.

Differential pulse voltammetry (DPV) has led in high sensitivity due to low capacitive current.[60] DPV of graphene/GCE was carried out in 0.1 M PBS to obtain the calibration curve of diuron. It could be observed that the peak currents increased upon increasing the concentration of diuron (**Figure 9**). A linear range (LR) was obtained in the range of 20 to 1000 μM with a regression equation of $y = 0.0062x + 4.1039$, ($R^2 = 0.998$). A low limit of detection (LOD), that is, 5 μM was also recorded, which was comparable with values reported in the literature. As compared with the analytical performance of carbon-based diuron sensors reported previously (**Table 2**), our electrode has promising outcomes with the wider LR and comparable LOD. Moreover, it is noteworthy that we used graphene without any further modifications.

The graphene/GCE exhibited excellent repeatability in four successive measurements with a relative standard deviation (RSD) of 3.82% calculated using peak currents. Similarly, the electrode offered good reproducibility by showing 5.17% of RSD, investigated on three different electrodes. The stability test of the electrode was conducted for a period of 2 weeks, which showed 4.21% RSD, indicating a satisfactory outcome for the stability of the electrode.

5. Conclusion

This work presents the synthesis of graphene from tea tree essential oil vapors in atmospheric pressure microwave plasma. The synthesis has been carried out in one step at a reasonably low microwave power of 200 W. The Raman spectra showed that the increase in microwave power raises the values of I_D/I_G ratio and FWHM of the 2D peak. XPS results revealed ≈87% of carbon and ≈10% of oxygen content, where oxygen is attached to the carbon in the form of hydroxyl and carbonyl functional groups. The signature of graphene was obtained using an XRD pattern, which showed 2θ at 23.6° and interlayer spacing of 0.37 nm. This is confirmed on HRTEM images as well. The impedance of graphene appeared to be less than half of bare GCE, indicating the fast electron-transfer kinetic

Table 2. Comparison of different carbon-based modified electrodes for electrochemical detection of diuron.

Electrode	Linear range	Limit of detection [μM]	Ref.
Nanocrystalline cellulose carbon paste electrode	4.2–47 μM	0.35	[57]
Nafion/AuNPs/RGO/GCE	1.0×10^{-6}–0.001 μM	4.1×10^{-7}	[61]
ITO-ppy-MWCNT-PSS polypyrrole	–	0.26	[62]
rGO–AuNPs/Nafion/GCE	0.001–0.1 μM	0.0003	[63]
MWCNT-COOH/GCE	0.215–2.15× μM	0.0688	[59]
MWCNT-COOH-MIP/carbon paste electrode	0.052–1.25 μM	0.009	[64]
Organometallic complexes and graphene oxide	50–1000 μM	20	[65]
GO-MWCNT/GCE	9–380 μM	1.49	[66]
Graphene/GCE	20–1000 μM	5	This work

behavior of graphene/GCE electrode. The graphene sensing performance for diuron herbicide was investigated by drop casting its aliquot on GCE. The graphene/GCE sensor showed a linear range from 20 to 1 mM, and a limit of detection of 5 μM.

Collectively, the produced graphene was equivalent in its purity and properties to graphene synthesized through any other methods. However, our methodology is superior in a way that it paves the way for green, energy-efficient, and fast synthesis route for graphene.

Acknowledgements

The authors thank the Centre for Microscopy and Microanalysis (CMM), the University of Queensland for XPS characterization. M.A.Z. gratefully acknowledges financial support through the Australian Government International Research Training Program Scholarship.

Open access publishing facilitated by James Cook University, as part of the Wiley - James Cook University agreement via the Council of Australian University Librarians.

Conflict of Interest

The authors declare no conflict of interest.

Data Availability Statement

The data that support the findings of this study are available from the corresponding author upon reasonable request.

Keywords

atmospheric pressure microwave plasma, graphene nanosheets, herbicide detection, sustainable precursor, tea tree oil

Received: November 25, 2022
Revised: January 17, 2023
Published online: March 3, 2023

[1] K. S. Novoselov, V. I. Fal'Ko, L. Colombo, P. R. Gellert, M. G. Schwab, K. Kim, *Nature* **2012**, *490*, 192.
[2] A. C. Ferrari, F. Bonaccorso, V. Fal'ko, K. S. Novoselov, S. Roche, P. Bøggild, S. Borini, F. H. L. Koppens, V. Palermo, N. Pugno, J. A. Garrido, R. Sordan, A. Bianco, L. Ballerini, M. Prato, E. Lidorikis, J. Kivioja, C. Marinelli, T. Ryhänen, A. Morpurgo, J. N. Coleman, V. Nicolosi, L. Colombo, A. Fert, M. Garcia-Hernandez, A. Bachtold, G. F. Schneider, F. Guinea, C. Dekker, M. Barbone, et al., *Nanoscale* **2015**, *7*, 4598.
[3] B. Yuyu, Z. Chen, W. Li, B. Hou, *ACS Appl. Mater. Interfaces* **2013**, *5*, 12361.
[4] P. P. Brisebois, M. Siaj, *J. Mater. Chem. C* **2020**, *8*, 1517.
[5] H. Wang, Q. Fu, C. Pan, *Electrochim. Acta* **2019**, *312*, 11.
[6] A. T. Smith, A. M. Lachance, S. Zeng, B. Liu, L. Sun, *Nano Mater. Sci.* **2019**, *1*, 31.
[7] N. Mcevoy, H. Nolan, N. Ashok Kumar, T. Hallam, G. S. Duesberg, *Carbon* **2013**, *54*, 283.
[8] A. Felten, A. Eckmann, J.-J. Pireaux, R. Krupke, C. Casiraghi, *Nanotechnology* **2013**, *24*, 355705.
[9] F. Hadish, S. Jou, B.-R. Huang, H.-A. Kuo, C.-W. Tu, *J. Electrochem. Soc.* **2017**, *164*, B336.
[10] A. Dato, M. Frenklach, *New J. Phys.* **2010**, *12*, 125013.
[11] E. Tatarova, A. Dias, J. Henriques, M. Abrashev, N. Bundaleska, E. Kovacevic, N. Bundaleski, U. Cvelbar, E. Valcheva, B. Arnaudov, A. M. B. Do Rego, A. M. Ferraria, J. Berndt, E. Felizardo, O. M. N. D. Teodoro, T.h. Strunskus, L. L. Alves, B. Gonçalves, *Sci. Rep.* **2017**, *7*, 10175.
[12] D. P. Hansora, N. G. Shimpi, S. Mishra, *JOM* **2015**, *67*, 2855.
[13] V. Agarwal, P. B. Zetterlund, *Chem. Eng. J.* **2021**, *405*, 127018.
[14] Y. Yan, F. Z. Nashath, S. Chen, S. Manickam, S. S. Lim, H. Zhao, E. Lester, T. Wu, C. H. Pang, *Nanotechnol. Rev.* **2020**, *9*, 1284.
[15] R. Kumar, R. K. Singh, D. P. Singh, *Renewable Sustainable Energy Rev.* **2016**, *58*, 976.
[16] D. H. Seo, A. E. Rider, Z. J. Han, S. Kumar, K. K. Ostrikov, *Adv. Mater.* **2013**, *25*, 5638.
[17] G. Ruan, Z. Sun, Z. Peng, J. M. Tour, *ACS Nano* **2011**, *5*, 7601.
[18] S. Sharma, G. Kalita, R. Hirano, Y. Hayashi, M. Tanemura, *Mater. Lett.* **2013**, *93*, 258.
[19] M. V. Jacob, R. S. Rawat, B.o Ouyang, K. Bazaka, D. S. Kumar, D. Taguchi, M. Iwamoto, R. Neupane, O. K. Varghese, *Nano Lett.* **2015**, *15*, 5702.
[20] A. Surjith, K. Bazaka, I. Levchenko, A. Al-Jumaili, B. Kandel, A. Alex, F. C. R. Hernandez, O. K. Varghese, M. V. Jacob, *ACS Appl. Mater. Interfaces* **2020**.
[21] T. Purkait, G. Singh, M. Singh, D. Kumar, R. S. Dey, *Sci. Rep.* **2017**, *7*, 15239.
[22] M. F. Malek, M. Robaiah, A. B. Suriani, M. H. Mamat, M. K. Ahmad, T. Soga, M. Rusop, S. Abdullah, Z. Khusaimi, M. Aslam, N. A. Asli, *J. Aust. Ceram. Soc.* **2021**, *57*, 347.
[23] A. N. Mohan, B. Manoj, *Chemistry* **2020**, *26*, 8105.
[24] C. Melero, R. Rincón, J. Muñoz, G. Zhang, S. Sun, A. Perez, O. Royuela, C. González-Gago, M. D. Calzada, *Plasma Phys. Controlled Fusion* **2017**, *60*, 014009.
[25] A. Dato, V. Radmilovic, Z. Lee, J. Phillips, M. Frenklach, *Nano Lett.* **2008**, *8*, 2012.
[26] A. Münzer, L. Xiao, Y. H. Sehlleier, C. Schulz, H. Wiggers, *Electrochim. Acta* **2018**, *272*, 52.
[27] K. Nakahara, J. Knego, T. Sloop, C. Bisquera, N. Subler, A. Dato, *Plasma Processes Polym.* **2020**, *17*, 1900244.
[28] D. Tsyganov, N. Bundaleska, A. Dias, J. Henriques, E. Felizardo, M. Abrashev, J. Kissovski, A. M. B. Do Rego, A. M. Ferraria, E. Tatarova, *Phys. Chem. Chem. Phys.* **2020**, *22*, 4772.
[29] O. Jašek, J. Toman, J. Jurmanová, M. Šnírer, V. Kudrle, V. Buršíková, *Diamond Relat. Mater.* **2020**, *105*, 107798.
[30] N. Bundaleska, D. Tsyganov, A. Dias, E. Felizardo, J. Henriques, F. M. Dias, M. Abrashev, J. Kissovski, E. Tatarova, *Phys. Chem. Chem. Phys.* **2018**, *20*, 13810.
[31] M. Jiménez, R. Rincón, A. Marinas, M. D. Calzada, *Int. J. Hydrogen Energy* **2013**, *38*, 8708.
[32] B. Liu, Z. Liu, I.-S. Chiu, M. Di, Y. Wu, J.-C. Wang, T.-H. Hou, C.-S. Lai, *ACS Appl. Mater. Interfaces* **2018**, *10*, 20237.
[33] K. Krishnamoorthy, M. Veerapandian, K. Yun, S. -J. Kim, *Carbon* **2013**, *53*, 38.
[34] L.u Shen, L. Zhang, K. Wang, L. Miao, Q. Lan, K. Jiang, H. Lu, M. Li, Y. Li, B. Shen, W. Zheng, *RSC Adv.* **2018**, *8*, 17209.
[35] C. R. S. V. Boas, B. Focassio, E. Marinho Jr., D. G. Larrude, M. C. Salvadori, C. R. Leão, D. J. dos Santos, *Sci. Rep.* **2019**, *9*, 13715.
[36] Y. Hao, Y. Wang, L. Wang, Z. Ni, Z. Wang, R. Wang, C. K. Koo, Z. Shen, J. T. L. Thong, *Small* **2010**, *6*, 195.

[37] R. Al-Gaashani, A. Najjar, Y. Zakaria, S. Mansour, M. A. Atieh, *Ceram. Int.* **2019**, *45*, 14439.
[38] T. N. Lambert, C. C. Luhrs, C. A. Chavez, S. Wakeland, M. T. Brumbach, T. M. Alam, *Carbon* **2010**, *48*, 4081.
[39] J. Toman, O. Jašek, M. Šnírer, D. Pavliňák, Z. Navrátil, J. Jurmanová, S. Chudják, F. Krčma, V. Kudrle, J. Michalička, *Plasma Processes Polym.* **2021**, *18*, 2100008.
[40] M. A. Zafar, M. V. Jacob, *Rev. Mod. Plasma Phys.* **2022**, *6*, 37.
[41] A. Al-Jumaili, M. A. Zafar, K. Bazaka, J. Weerasinghe, M. V. Jacob, *Tanso Sen'i no Saisentan Gijutsu* **2022**, *7*, 100157.
[42] J. Bao, V. Giurgiutiu, *Proc. SPIE* **2013**, *8695*, 869521.
[43] G. Chilkoor, K. Jawaharraj, B. Vemuri, A. Kutana, M. Tripathi, D. Kota, T. Arif, T. Filleter, A. B. Dalton, B. I. Yakobson, M. Meyyappan, M. M. Rahman, P. M. Ajayan, V. Gadhamshetty, *ACS Nano* **2020**, *14*, 14809.
[44] Y. Wang, Z. Su, W. Wu, S. Nie, X. Lu, H. Wang, K. Mccarty, S.-S. Pei, F. Robles-Hernandez, V. G. Hadjiev, J. Bao, *Nanotechnology* **2014**, *25*, 335201.
[45] H. A. Calderon, F. Alvarez Ramirez, D. Barber, V. G. Hadjiev, A. Okonkwo, R. Ordoñez Olivares, I. Estrada Guel, F. C. Robles Hernandez, *Carbon* **2019**, *153*, 657.
[46] H. A. Calderon, I. Estrada-Guel, F. Alvarez-Ramírez, V. G. Hadjiev, F. C. Robles Hernandez, *Carbon* **2016**, *102*, 288.
[47] H. A. Calderon, A. Okonkwo, I. Estrada-Guel, V. G. Hadjiev, F. Alvarez-Ramírez, F. C. Robles Hernández, *Adv. Struct. Chem. Imaging* **2016**, *2*, 10.
[48] G. Wang, X. Shen, B. Wang, J. Yao, J. Park, *Carbon* **2009**, *47*, 1359.
[49] H. Asgar, K. M. Deen, U. Riaz, Z. U.r Rahman, U. H. Shah, W. Haider, *Mater. Chem. Phys.* **2018**, *206*, 7.
[50] W. Chen, D. Li, L.i Tian, W. Xiang, T. Wang, W. Hu, Y. Hu, S. Chen, J. Chen, Z. Dai, *Green Chem.* **2018**, *20*, 4438.
[51] E. Tatarova, J. Henriques, C. C. Luhrs, A. Dias, J. Phillips, M. V. Abrashev, C. M. Ferreira, *Appl. Phys. Lett.* **2013**, *103*, 134101.
[52] R. Rincón, C. Melero, M. Jiménez, M. D. Calzada, *Plasma Sources Sci. Technol.* **2015**, *24*, 032005.
[53] A. Casanova, R. Rincón, J. Muñoz, C. O. Ania, M. D. Calzada, *Fuel Process. Technol.* **2021**, *212*, 106630.
[54] M. Singh, A. Sengupta, K. Zeller, G. Skoptsov, R. L. Vander Wal, *Carbon* **2019**, *143*, 802.
[55] M. A. Zafar, Y. Liu, S. Allende, M. V. Jacob, *Tanso Sen'i no Saisentan Gijutsu* **2022**, *8*, 100188.
[56] S. Allende, Y. Liu, M. A. Zafar, M. V. Jacob, *Waste Disposal & Sustainable Energy* **2023**.
[57] M. Serge, K. Yssouf, B. Y. F. Roland, T. Issa, S. Fadilatou, K. Bazoumana, S. Irenée, T. K. Ignas, N. Emmanuel, *Int. J. Electrochem. Sci.* **2021**, *16*, 210552.
[58] A. Wong, M. R. De Vasconcelos Lanza, M. D. P. T. Sotomayor, *J. Electroanal. Chem.* **2013**, *690*, 83.
[59] I. M. Morita, G. M. Araújo, L. Codognoto, F. R. Simões, *Int. J. Environ. Anal. Chem.* **2019**, *99*, 1565.
[60] L. C. Brazaca, L. Ribovski, B. C. Janegitz, V. Zucolotto, in *Medical Biosensors for Point of Care (POC) Applications* (Ed.: R. J. Narayan), Elsevier, Amsterdam, the Netherlands **2017**, pp. 229–254.
[61] J. Qin, *Int. J. Electrochem. Sci.* **2020**, *15*, 11203.
[62] G. M. De Araújo, F. R. Simões, *J. Solid State Electrochem.* **2018**, *22*, 1439.
[63] K. Zarei, A. Khodadadi, *Ecotoxicol. Environ. Saf.* **2017**, *144*, 171.
[64] A. Wong, M. V. Foguel, S. Khan, F. M. D.e Oliveira, C. R. T. Tarley, M. D. P. T. Sotomayor, *Electrochim. Acta* **2015**, *182*, 122.
[65] A. Wong, M. D. P. T. Sotomayor, *J. Electroanal. Chem.* **2014**, *731*, 163.
[66] V. Mani, R. Devasenathipathy, S.-M. Chen, T.-Y. Wu, K. Kohilarani, *Ionics* **2015**, *21*, 2675.